JOM
https://doi.org/10.1007/s11837-024-06470-0

Leaching Kinetics of Limonite-Type Laterite Nickel Ore from Ammonium Hydrogen Sulfate Solution at Atmospheric Pressure

YI WANG,[1] YUSHENG WU,[1,2] YING FAN,[1] YUZHENG WANG,[1] and LAISHI LI[1,3]

1.—School of Materials Science and Engineering, Shenyang University of Technology, Shenyang 110870, China. 2.—e-mail: wuyus@sut.edu.cn. 3.—e-mail: lilaishi@sut.edu.cn

The leaching behavior of nickel and iron in limonite-type laterite nickel ore was studied through ammonium hydrogen sulfate atmospheric leaching. The leaching temperature, ammonium bisulfate concentration, reaction time, and acid excess rate during the nickel dissolution process were optimized using the response surface methodology (RSM) Box–Behnken design. The parameters of the optimal process conditions obtained are 74% mass concentration of NH_4HSO_4, 83 min leaching time, 17% excess of NH_4HSO_4, and 112°C leaching temperature, and the maximum recovery of nickel is 90.9%. The kinetic behavior of nickel and iron leaching processes was evaluated using a shrinking core model, and their activation energies were calculated. The results show that the kinetic models for the leaching of nickel and iron are consistent with the chemical reaction model, which can be expressed by the linear equation $1 - (1 - \alpha)^{1/3} = k_r t$. Based on the linear equation and Arrhenius equation, the activation energies of leached nickel and iron are 67.76 kJ/mol and 68.81 kJ/mol, respectively.

INTRODUCTION

As the expansion of the global market economy has accelerated recently, a new energy industry has ushered in a period of rapid development. Nickel, as the key metal in new energy vehicle power batteries, is known as the white oil of the twenty-first century, and its demand is rising. Therefore, the effective extraction of nickel is crucial to the advancement of the sustainable growth of the new energy industry worldwide.[1]

According to data published by the Geological Survey (USGS) in 2021, nickel resources are classified into two categories according to the different forms of nickel in the ore: sulfide nickel ore and laterite nickel ore.[2] Due to the sharp increase in demand for nickel and the decline in global sulfide nickel reserves, laterite nickel is now an important source of nickel extraction.[3] At present, nickel and iron can be extracted from laterite nickel ore using two different processes: hydrometallurgy and pyrometallurgy. Limonitic laterite nickel ore is more suitable for hydrometallurgical processes.[4] Common hydrometallurgical processes include high-pressure acid leaching (HPAL),[5,6] atmospheric pressure acid leaching (AL),[7–9] and ammonia leaching (Caron).[10,11] Li et al.,[12] studied the kinetic hydrochloric acid atmospheric pressure leaching of laterite ore. Synthetic leaching mechanisms for various minerals at various times were created. The kinetic model of diffusion control is adequate, as demonstrated by the kinetic study of the leaching processes for nickel, cobalt, and manganese. He et al.,[6] investigated the nitric acid pressurized leaching (NAPL) of limonite laterite using an autoclave equipped with an acid injection and sample extraction system to study the precipitation behavior of nickel, iron, and minerals during the leaching process. Then, a kinetic model for the nickel dissolution process was derived. The results showed that temperature, acid concentration, and liquid-solid ratio were positively correlated with nickel

(Received November 9, 2023; accepted February 19, 2024)

Published online: 13 March 2024

extraction. Nasab et al.,[13] conducted research on the kinetics of extracting nickel and cobalt from iron-rich laterite ores using sulfuric acid at atmospheric pressure. The results showed that a strong temperature dependence of the leaching process indicates chemical control. Prameswara et al.,[14] investigated the kinetics and optimization of nickel recovery from Morowali laterite ore leaching with sulfuric acid using the shrinking core model and the Zhuravlev, Leshokin, and Templeman (ZLT) model to evaluate the kinetics of the nickel leaching process. The maximum nickel recovery of 85% was noted, and 32.78 kJ/mol was found to be the apparent activation energy. According to earlier research, the most appropriate kinetic model for explaining the leaching of metal ions is thought to be the Shrinking Core Model (SCM).[12–14] Numerous studies have concluded that the most studied processes are those that involve sulfuric acid leaching. For example, the sulfuric acid pressurized leaching (PAL) process and the sulfuric acid high-pressure leaching (HPAL) process are the preferred methods for the leaching of nickel and iron from limonitic laterites, and these processes have the advantage that iron can be precipitated in the form of hematite.[15,16] However, the PAL and HPAL processes have relatively high operating costs compared to sulfuric acid atmospheric leaching (AL), require significant investment, are energy intensive, and have large amounts of residual acid at commercial levels.[17] Although the existing hydrometallurgical process of atmospheric pressure leaching (AL) of sulfuric acid has low energy consumption and is environmentally friendly, it also suffers from the disadvantages of complex process routes, high requirements for equipment process conditions, and poor material recycling.[18]

Therefore, the development of new and more economical process technologies for low-grade limonite-type laterite nickel ores is currently a hot issue in industry research. The benefits of ammonium bisulfate leaching are as follows: (1) low leaching temperature (< 120°C) and gentle reaction conditions The ammonium bisulfate solution has a modest acidity, the requirements for equipment are low, and the whole leaching process will not produce wastewater or exhaust gas, which has high prospects for industrial applications. (2) The leaching agent (NH_4HSO_4) can be recycled, which helps to reduce the consumption of reagents, and the process is simple with low energy consumption, which can realize the effective separation of metallic nickel. (3) By heating and reacting nickel-containing ores with ammonium bisulfate, the nickel-iron metal components and silicon are separated, and then iron is removed with ammonia, and then coarse particles of nickel hydroxide with a good separation effect are prepared in the precipitation reaction device. However, the relevant basic research on this technology is relatively small, and some key problems still need to be solved. Considering the aforementioned benefits, this study offers the first comprehensive investigation into the atmospheric pressure leaching of laterite nickel ores of the limonite type using an ammonium bisulfate solution. Our group previously used ammonium persulfate leaching of fly ash[19] and low-grade magnesite,[20] both of which achieved better results. This study was carried out at atmospheric pressure, which is milder compared to the experimental conditions of ammonium bisulfate high-pressure leaching of fly ash, further proving the feasibility of this method. da Silva et al.,[3] investigated the precipitation strategy of iron in sulfate leach solution of laterite nickel ores, where iron was effectively removed from sulfate leach solution containing nickel and cobalt by chemical precipitation using NH_4OH and milk of lime as precipitants. The final solution contained only 2.1 mg/L of iron, and the loss of nickel and cobalt was < 1.6%. Liu et al.,[21] investigated the recovery of cobalt and nickel from magnesium-rich sulfate leach solution by the magnesium oxide precipitation method, and the present work demonstrated that the magnesium oxide precipitation method is capable of precipitating and separating nickel and cobalt in the magnesium-rich sulfate leach solution of nickel oxide ores. Equilibrium pH is essential to maximize nickel and cobalt pre-precipitation and reduce magnesium precipitation, which in the pre-precipitates can be readily dissolved in low-acid sulfuric acid solutions and separated from magnesium. The results showed that different concentrations of iron helped the co-extraction of cobalt. Astuti et al.,[22] investigated a new method: oxalate precipitation for the extraction of nickel and cobalt from citrate leach of laterite nickel ores. The proposed method includes an oxalate precipitation step for the precipitation of nickel (and cobalt) from the citrate leach filtrate, and the experimental results of the oxalate precipitation show that complete precipitation of nickel can be achieved at 80°C, and that the method produces mixed oxalate precipitation (MOP) with a purity of 78% precipitation (MOP) with a purity of 78%. It can be summarized from many studies that nickel can be recovered in acidic leaching solutions such as sulfuric acid at present, and this thesis is also in the same acidic system; therefore, this thesis can also achieve the separation of metallic elements such as nickel and iron and the recovery of nickel from the leaching solution by adjusting the pH value in the leaching solution.

In this study, to determine and optimize the optimal processing conditions, a thorough kinetic analysis is necessary to further determine the leaching mechanism of ammonium bisulfate solutions. The response surface methodology was used in this paper's kinetic analysis of the dissolution process to analyze the type of kinetic model and activation energy based on single-factor experiments. This analysis helped determine the ideal process conditions and optimized the dissolution

process's effective parameters, including the leaching temperature, ammonium bisulfate concentration, reaction time, and acid excess rate.

EXPERIMENTAL

Materials and Pretreatment

The limonite-type laterite nickel ore used in this experiment was provided by Ningbo Liqin Resource Technology Co., Ltd., from Indonesia, which is a reddish-brown clay-like mineral. The main chemical composition of limonite-type laterite nickel ore was determined by x-ray fluorescence (XRF), and the results are shown in Table I. This type of laterite sample is rich in nickel and cobalt, low in magnesium, and high in iron. The nickel laterite sample was sieved and vacuum dried overnight at 105°C before the ore was ground until 100% passed through a 100-μm sieve. Analytical-grade ammonium bisulfate was acquired from Sinopharm Chemical Reagent Co. The trials used distilled water.

Experimental Method

The complete process flow of ammonium bisulfate leaching of limonite-type laterite nickel ore is shown in supplementary Fig. S-1 (refer to online supplementary material). The leaching experiments were carried out in a three-necked flask equipped with a reflux condenser to prevent evaporation of the liquid during the heating process. First, 10 g of raw laterite nickel ore sample was weighed with an electronic balance, and ammonium bisulfate was dissolved in deionized water at a certain stoichiometric ratio to obtain a certain mass concentration of ammonium bisulfate solution. A total of 10 g of laterite nickel ore and ammonium bisulfate solution with a certain stoichiometric ratio were put into a three-necked flask and mixed homogeneously. They were then placed in a temperature-controlled magnetic stirring water bath equipped with a digitally controlled thermometer (within the range of $\pm$ 0.5°C), adjusted the temperature of the constant-temperature water bath to reach the test temperature and then stirred immediately.

When limonitic laterite nickel ore was leached by ammonium bisulfate solution, the following chemical reactions occurred with the metal oxide in laterite nickel ore:

$$NiO(s) + 2NH_4HSO_4(aq) = (NH_4)_2Ni(SO_4)_2(aq) + H_2O(l) \quad (1)$$

$$MgO(s) + 2NH_4HSO_4(aq) = (NH_4)_2Mg(SO_4)_2(aq) + H_2O(l) \quad (2)$$

$$MnO(s) + 2NH_4HSO_4(aq) = (NH_4)_2Mn(SO_4)_2(aq) + H_2O(l) \quad (3)$$

$$Fe_2O_3(s) + 6NH_4HSO_4(aq) = 2NH_4Fe(SO_4)_2(aq) + 2(NH_4)_2SO_4(aq) + 3H_2O(l) \quad (4)$$

$$Al_2O_3(s) + 6NH_4HSO_4(aq) = 2NH_4Al(SO_4)_2(aq) + 2(NH_4)_2SO_4(aq) + 3H_2O(l) \quad (5)$$

After a predetermined leaching time, the reaction was stopped, and the leached slurry in the three-necked flask was placed in a Brinell's funnel, and vacuum filtration was carried out to realize solid-liquid separation to obtain leaching residue and leaching solution. The three-necked flask was rinsed with a certain amount of ultrapure water, and the filter residue was washed three times with deionized water and finally dried in an oven at 105°C. The leached residue was milled, characterized, and analyzed.

A comprehensive study was conducted on the effects of different process conditions on nickel extraction, and the leaching rate was calculated. The results can be obtained from Eq. 6:

$$\varphi = \frac{(M_1/S_1) - (M_2/S_2)}{(M_1/S_1)} \quad (6)$$

where φ denotes the Ni^{2+}/Fe^{3+} leaching rate, and (M_1/S_1) and (M_2/S_2) denote the mass ratio of NiO/Fe_2O_3 to SiO_2 in the raw laterite nickel ore and leaching residue, respectively.

The kinetic analysis is based on experimental data on nickel dissolution. The kinetic experiment was conducted under the following reaction conditions: by changing temperature and time, the kinetic experiment was conducted with the optimal values of three parameters (NH_4HSO_4 mass

Table I. Chemical composition of laterite sample (mass fraction, %)

Compound	Fe_2O_3	Al_2O_3	SiO_2	MgO	Cr_2O_3	NiO	MnO	Na_2O	Co_3O_4	Others	LOI
Wt%	65.42	5.38	5.15	3.72	4.55	1.56	1.38	0.49	0.16	0.58	11.61

concentration, NH_4HSO_4 excess rate, and stirring speed). The leaching temperatures of 75–115°C as well as the leaching times of 10–90 min were studied, and at the end of the reaction time, the contents of the reaction vessel were filtered with vacuum filters for filtration, respectively, and the leached residue was ground, dried, and then characterized and analyzed. All experiments were repeated three times for all leaching temperatures and different reaction times, and the results of the leaching rate were averaged.

Material Characterization

In this paper, the chemical composition of dried laterite ore was analyzed using x-ray fluorescence spectrometry (XRF, ARL PERFORM'X Thermo Fisher Scientific, USA). Mineralogical studies of the main minerals were carried out using x-ray diffraction (XRD, XRD-7000X, Shimadzu, Japan) with Cu Kα radiation ranging from 10° to 70° (2θ). Surface morphology and composition of nickel laterite were obtained using a Zeiss thermal field scanning electron microscope (SEM, GeminiSEM300, Germany) equipped with an energy-dispersive x-ray spectrometer (EDS, Oxford Instruments, UK).

RESULTS AND DISCUSSION

Mineralogical Analysis

Table I shows that the contents of NiO, Fe_2O_3, and MgO in laterite nickel ore are 1.56%, 65.42%, and 3.72%, respectively, and the samples have high iron content and low nickel and magnesium content, which are typical of limonite-type laterite nickel ore. Figure 1a shows the XRD pattern of the original minerals, which clearly indicates that the main physical phase composition of limonite-type lateritic nickel ores is needle ferrite (FeO(OH)), hematite (Fe_2O_3), quartz (SiO_2), pyrophyllite($Al_2Si_4O_{10}(OH)_2$), and spinel ($FeNiO_4$), where nickel exists mainly in the form of nickel-iron oxides in lateritic nickel ores.

The surface morphology of nickel laterite analyzed by SEM (GeminiSEM300) and EDS (EDS, Oxford instruments) is shown in Fig. 1b and c. The results show that the surface roughness of laterite nickel ore mainly consists of large mass particles, and the surface morphology is mainly in the form of needles, grains, veins, and irregularities. The main elements present on the surface are Fe, Ni, Mg, Al, and Si.

Optimization of Influential Parameters for Maximizing the Ni

Design Expert 13 (DX13) software was chosen to design the experiments, reduce the number of experiments, optimize the experiments, and study the relationship between the parameters.[23,24]

The analysis of the ammonium bisulfate leaching of laterite nickel ores shows that each factor has different effects on the experiment. To carry out a systematic study, a comprehensive condition test is needed. Based on the literature and preliminary experiments, many studies have been conducted to understand how different process variables affect nickel extraction. In this experiment, there were four independent variables, namely, ammonium bisulfate concentration (A, %), leaching time (B, min), ammonium bisulfate excess rate (C, %), and leaching temperature (D, °C). The dependent variable was nickel leaching rate (Y). The design of the experiment was analyzed by Design-Expert software. Table II shows the range of values of the independent variables. Twenty-nine CCD experiments were conducted through a central composite design. Supplementary Table S-1 shows the responses obtained by selecting four parameters and each experimental condition at three different levels to examine their impact on nickel dissolution. In this study, the high acid consumption was due to the high iron content in the laterite samples. It should be noted that the average particle size and stirring speed were the optimal fixed values in these experiments.

In ANOVA, the P-value is an indicator used to measure the difference between the control group and the experimental group. The larger the F-value, the value of $P > F$ is < 0.05 in ANOVA, indicating that the model term has a significant impact on the response.[25] Table III shows the analysis of variance (ANOVA). Each of these four parameters had a significant effect on the leaching rate of nickel, and the F-value of the model was 135.15; hence, the model was significant. The R^2 value in this study is 0.9927, demonstrating a good correlation between the experimental and predicted values of nickel leaching rate. The leaching temperature has the greatest effect on the nickel leaching rate, with the highest F value of 1250.41. The effects of ammonium bisulfate concentration (A, %), leaching time (B, min), ammonium bisulfate excess rate (C, %), leaching temperature (D, °C), and AD, BC, BD, B^2, C^2, and D^2 were statistically significant and important modeling terms in this experiment. The more significant the variable's response is, the higher the mean square value. As a result, $D > B > A > D^2 > B^2 > C > C^2 > BD > BC > AD$ is the validity ranking for the significant model terms. The model is adjusted, and the resultant equation is displayed in Eq. 7 after the irrelevant terms with P-values > 0.05 are eliminated:

$$Y = 58.89 + 10.93 * A + 11.55 * B + 3.55 * C + 24.97 * D + 2.67 * AD + 2.96 * BC + 3.35 * BD - 6.11 * B^2 - 3.94 * C^2 - 7.03 * D^2 \quad (7)$$

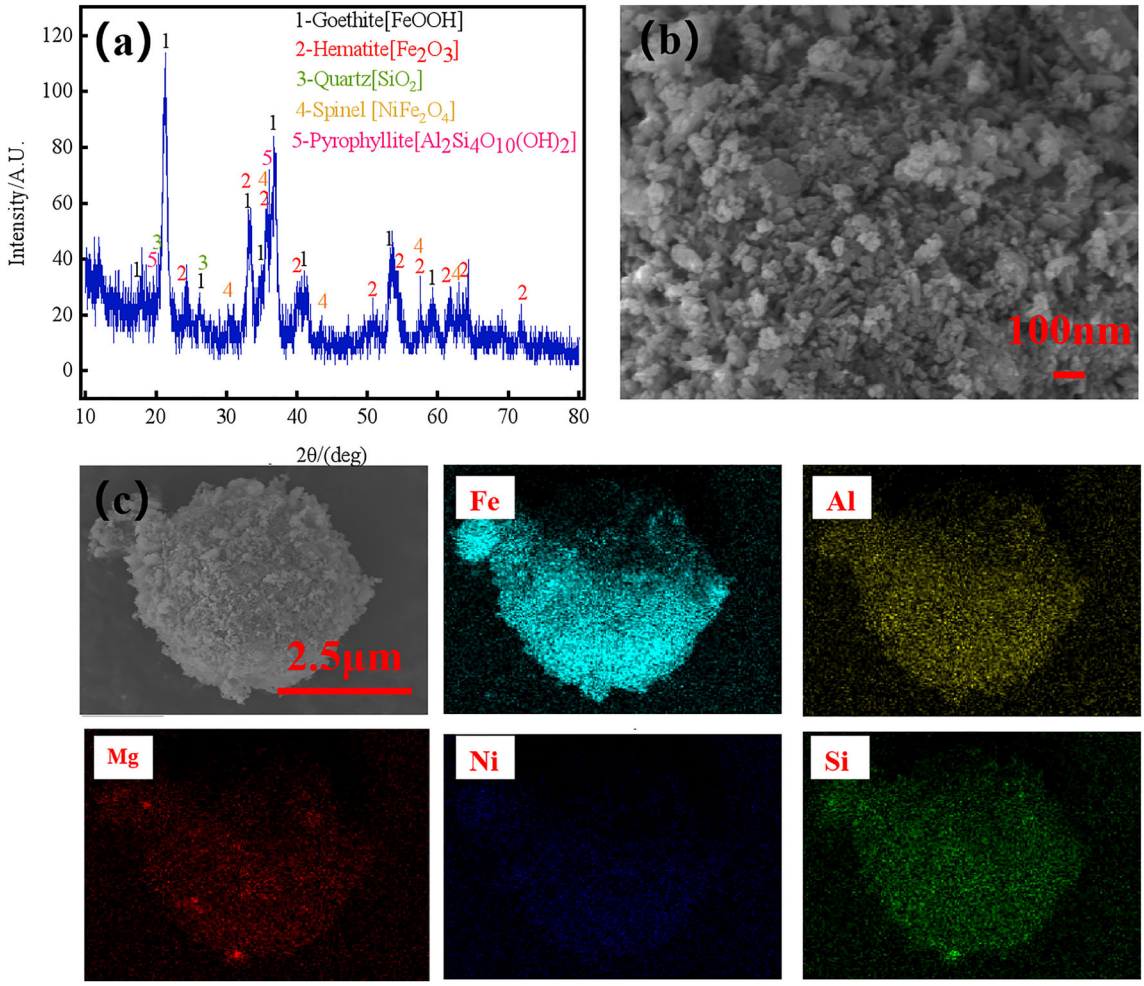

Fig. 1. XRD (a), SEM images (b), and EDS (c) spectral analysis of the laterite nickel ore.

From Eq. 7, the contribution of leaching temperature is greater than that of the other factors and has a positive effect; the contribution of reaction time, acid concentration, and acid excess are positively affected; the impact of acid excess on nickel leaching rate is minimal. The positive coefficients in this equation indicate positive effects, and the negative coefficients indicate negative effects on the nickel leaching rate. This result is the same as that of nickel recovery, and the actual and predicted values of nickel dissolution are shown in Fig. 2.

Figure 3 shows the three-dimensional model obtained according to Eq. 7. The model shows that the leaching temperature has the greatest effect on the leaching rate of nickel, the leaching time and acid concentration have relatively small effects on the leaching rate of nickel, and the acid excess rate has the least effect on the leaching rate of nickel. Figure 3a shows that the maximum leaching rate of nickel is 89% when the concentration of ammonium bisulfate solution is 75% and the temperature is 115°C. The leaching rate of nickel increased with increasing leaching temperatures and acid concentrations. At a leaching temperature of 95°C, an acid excess of 30%, and a reaction time of 90 min, the nickel leaching rate increased from 52.95% to 75.96% by increasing the acid concentration rate from 45% to 75%. At a leaching temperature of 95°C, an acid excess of 30%, and an acid concentration of 75%, the nickel leaching rate was increased from 51.73% to 75.96% by increasing the reaction time from 30 min to 90 min. The difference in nickel leaching rate increase is basically the same within each time range and each leaching concentration range. During the leaching process, a higher concentration of ammonium bisulfate solution was not used because the nickel leaching rate did not significantly improve. As a result, the optimal concentration of ammonium bisulfate identified in this study was 75%.

Figure 3b shows that the leaching rate of nickel increased significantly with increasing leaching temperature and leaching time, and at a reaction time of 90 min, the leaching rate of nickel at leaching temperatures of 75–115°C increased significantly. In each temperature range, the difference in increase was greater than at shorter leaching times. During the 90 min leaching process,

Table II. Center composite design experiment arrangement and results

	Independent variable				
No.	***A* (%)**	***B* (min)**	***C* (%)**	***D* (°C)**	**Recovery Ni (%)**
1	45	30	30	95	33.02
2	75	30	30	95	51.73
3	45	90	30	95	52.95
4	75	90	30	95	75.96
5	60	60	10	75	20.72
6	60	60	50	75	24.92
7	60	60	10	115	70.69
8	60	60	50	115	79.44
9	45	60	30	75	21.85
10	75	60	30	75	35.55
11	45	60	30	115	65.22
12	75	60	30	115	89.59
13	60	30	10	95	36.07
14	60	90	10	95	57.3
15	60	30	50	95	37.61
16	60	90	50	95	70.68
17	45	60	10	95	38.67
18	75	60	10	95	64.65
19	45	60	50	95	46.35
20	75	60	50	95	71.68
21	60	30	30	75	15.41
22	60	90	30	75	28.76
23	60	30	30	115	57.58
24	60	90	30	115	84.35
25	60	60	30	95	58.36
26	60	60	30	95	57.34
27	60	60	30	95	61.96
28	60	60	30	95	60.34
29	60	60	30	95	62.99

Table III. Analysis of variance for nickel dissolution in the acid-leaching process

Source	**Sum of squares**	***df***	**Mean square**	***F* valued**	***P*-value**	
Model	11,323.41	14	808.81	135.15	< 0.0001	Significant
A-Acid concentration	1432.27	1	1432.27	239.33	< 0.0001	
B-Time	1600.37	1	1600.37	267.42	< 0.0001	
C-Acid excess	151.09	1	151.09	25.25	0.0002	
D-temperature	7483.01	1	7483.01	1250.41	< 0.0001	
AB	4.62	1	4.62	0.7724	0.3943	
AC	0.1056	1	0.1056	0.0176	0.8962	
AD	28.46	1	28.46	4.76	0.0467	
BC	35.05	1	35.05	5.86	0.0297	
BD	45.02	1	45.02	7.52	0.0159	
CD	5.18	1	5.18	0.8648	0.3681	
A^2	1.48	1	1.48	0.2474	0.6266	
B^2	249.56	1	249.56	41.70	< 0.0001	
C^2	105.49	1	105.49	17.63	0.0009	
D^2	328.85	1	328.85	54.95	< 0.0001	
Residual	83.78	14	5.98			
Lack of fit	61.32	10	6.13	1.09	0.5086	Not significant
Pure error	22.47	4	5.62			
Cor total	11,407.19	28				

the leaching rate of nickel varies between 20.72% and 70.69% within the leaching temperature range of 75–115°C. The nickel leaching rate is mostly determined by the leaching temperature. The number of activated molecules increases as the temperature rises because the reactant's molecular mobility in the reaction system accelerates. The system experiences a higher number of atom-molecule collisions, which quickens the rate at which the process leaches.

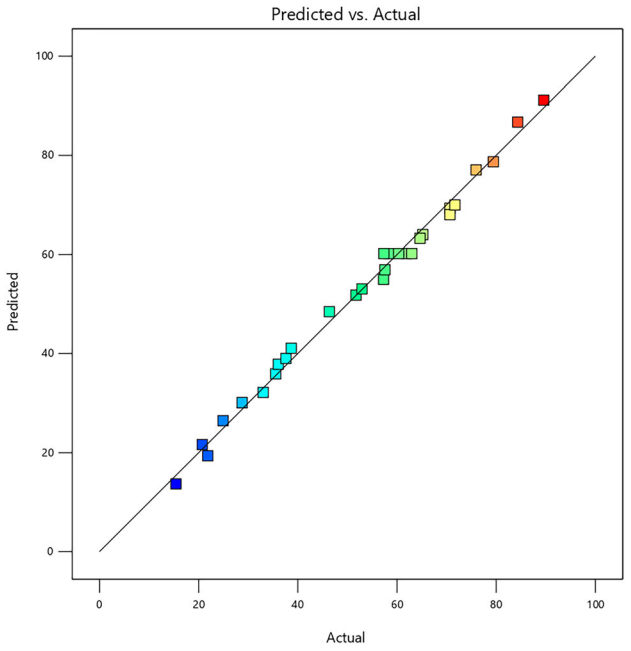

Fig. 2. The actual versus predicted values of Ni dissolutions.

Figure 3c shows that with the increase in acid excess rate and leaching time, the nickel leaching rate slightly increases. At a leaching temperature of 95°C, a leaching time of 60 min, and an acid concentration of 75%, the nickel leaching rate was increased from 64.65% to 71.68% by increasing the acid excess rate from 10% to 50%. This indicates that the acid excess rate has minimal impact on the nickel leaching rate. According to Ref. 26, when the slurry has a high solid-liquid ratio, a low leaching rate occurs because the slurry becomes viscous and inhibits ion migration. This may also be due to insufficient H^+ ion concentration to leach the available solids. Similarly, at a leaching temperature of 95°C, an acid excess of 30%, and an acid concentration of 75%, and extending the leaching time from 30 min to 90 min, the nickel leaching rate increased from 51.73% to 75.96%. This indicates that, compared to the effect of acid excess rate, reaction time has a greater impact on nickel leaching rate. At 75–90 min, the range of increase in nickel leaching rate decreases, and the optimal leaching time is 90 min. Reference 27 also mentioned that the nickel leaching rate increased slightly in the leaching duration range of 60–120 min. However, at the beginning of the leaching process (0–30 min), the nickel leaching rate increased significantly.

According to software calculations, during the process of leaching laterite samples with

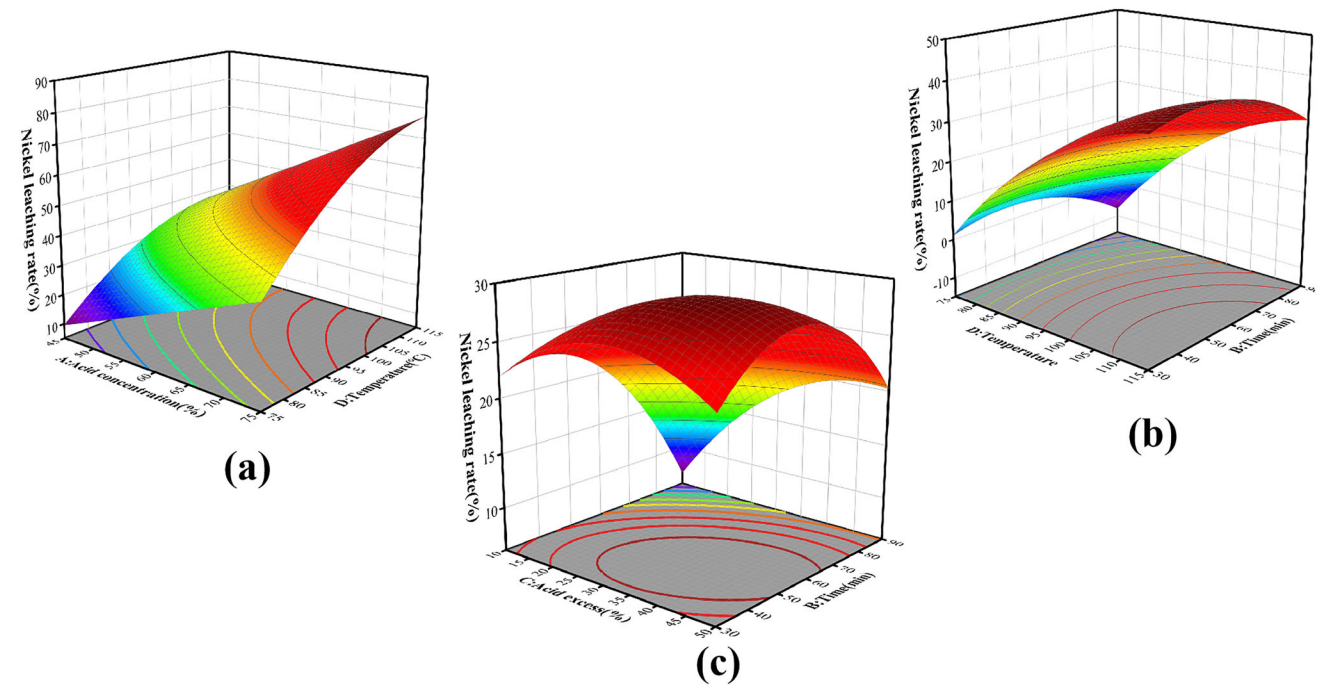

Fig. 3. Three-dimensional response surface plot. (a) The effect of temperature and acid concentration on the leaching rate of elemental nickel. (b) The effect of time and temperature on the leaching rate of elemental nickel. (c) The effect of time and acid concentration on the leaching rate of elemental nickel.

ammonium bisulfate, the optimal parameters for the highest nickel leaching rate are given as follows: ammonium bisulfate concentration: 74%, leaching time: 83 min, acid excess rate of 17%, and leaching temperature of 112°C. According to software calculations, the highest leaching rate of nickel is 90.9%, which is consistent with the experimental results.

Effect of Temperature and Time on the Leaching Rate of Nickel and Iron

The kinetic tests were performed by varying the temperature and time at the optimum values of the above parameters. As shown in Fig. 4a and b, from 75°C to 115°C, the higher the leaching temperature and the longer the reaction time, the faster the leaching rate of nickel and iron and the higher the final leaching rate obtained, which suggests that increasing the leaching temperature and prolonging the reaction time are favorable to the extraction of nickel and iron. At the beginning of leaching, the extraction speed was very fast. Within the first 20 min, the nickel leaching rate reached 78.51%, and the iron leaching rate reached 67.1%. At 115°C, the nickel leaching rate peaked in the shortest time compared to lower temperatures. Figure 4a and b shows that when the temperature rises from 75°C to 115°C, the leaching temperature increases by 40°C. After 90 min of leaching, the leaching rates of nickel and iron increase by almost 2.5 times. The leaching rate of nickel increased by 9.73% compared to that of iron; thus, the leaching rate of nickel is more sensitive to temperature than that of iron. After 75 min, the dissolution rate of nickel and iron slightly increased. To improve the leaching rate of nickel and iron, the optimal reaction time and leaching temperature were 90 min and 115°C. Thus, the highest leaching rates of nickel and iron, 88.96% and 79.23%, respectively, were obtained using ammonium bisulfate at a concentration of 75%, an acid excess of 50%, a leaching temperature of 115°C, and a reaction time of 90 min.

Leaching Kinetics of Nickel and Iron

The shrinking-core model was selected in this study because it is more appropriate for the leaching of nonporous solids, given that the ore is primarily composed of dense particles that are classified as nonporous particles and that the ore particles gradually shrink during the leaching process, forming a product layer around the unreacted particles.[28] The reaction steps of the leaching process for the shrink-core model include (1) outward diffusion of liquid reactants or products through the liquid boundary layer and (2) liquid reaction models, such as homogeneous, granular, and pore models, are usually applied to porous solid-liquid systems. The reactants or products occur diffusely through the interior of the solid product layer and (3) chemical interactions at the interface. The control stage in the reaction process is the slowest. Stated differently, the three types of control processes are mixing control, diffusion control, and chemical reaction control. One can categorize diffusion control into two groups: internal diffusion control and external diffusion control. Equations 8, 9, and 10 are used to represent the kinetic equations when external diffusion, internal diffusion, and chemical reaction are controlling the reaction process, respectively.[29]

$$[1-(1-a)^{1/3}]^2 = K_d t \tag{8}$$

$$1-3*(1-a)^{2/3}+2*(1-a) = K_d t \tag{9}$$

$$1-(1-a)^{1/3} = K_r t \tag{10}$$

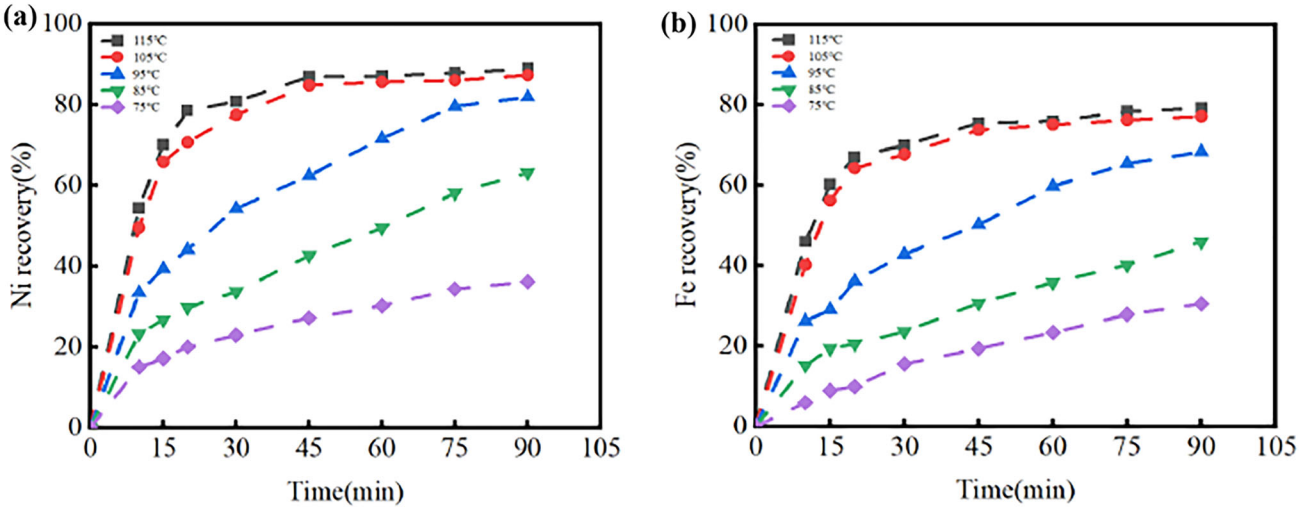

Fig. 4. Recovery of (a) nickel and (b) iron at different temperatures and times under optimal conditions (ammonium bisulfate concentration: 75%, acid excess rate: 50%).

where the "diffusion rate constant" is k_d (min^{-1}) and the "reaction rate constant" is k_r (min^{-2}). A is the fraction of nickel dissolved at time t.

The two shrinkage kernel model models with Eqs. 9 and 10 of control of diffusion through the interior of the product layer and chemical control provided the best fit to the nickel and iron leaching data in the species studied. Kinetic modeling of surface chemical control and internal diffusion control reactions for the extraction of nickel and iron from leaching of laterite nickel ores with ammonium bisulfate solution at different temperatures should be shown in Fig. 5, respectively. The first part of Fig. 5 has the highest slopes (highest reaction rate constants), and these slopes (values of the reaction rate constants) were used to determine the activation energies. Table IV shows the reaction rate constants and correlation coefficients for nickel and iron dissolution at different temperatures. The chemical control model gives a better fit compared to the internal diffusion model, especially for nickel. This was shown using the Arrhenius Eqs. 11 and 12:

$$K_d = A * \exp(-E_a/RT) \tag{11}$$

$$\ln K_d = \ln A - E_a/RT \tag{12}$$

where A is the frequency factor (s^{-1}), E_a is the apparent reaction activation energy (kJ/mol), R is the molar gas constant (kJ/mol k), and T is the thermodynamic temperature (k).

The two control models were plotted, and then the activation energy values were calculated. These graphs and correlation coefficient values for nickel and iron leaching are given in Fig. 6. The correlation coefficients R^2 for iron and nickel, which are employed for chemical control, are satisfactory at 0.9445 and 0.9715, respectively, as shown in Fig. 6a and b. Using the Arrhenius relationship, the activation energies for the chemical control model's dissolution of nickel and iron are demonstrated to be, respectively, as follows:

$$E_a = 67.76 \text{ kJ/mol}$$
$$E_a = 68.81 \text{ kJ/mol}$$

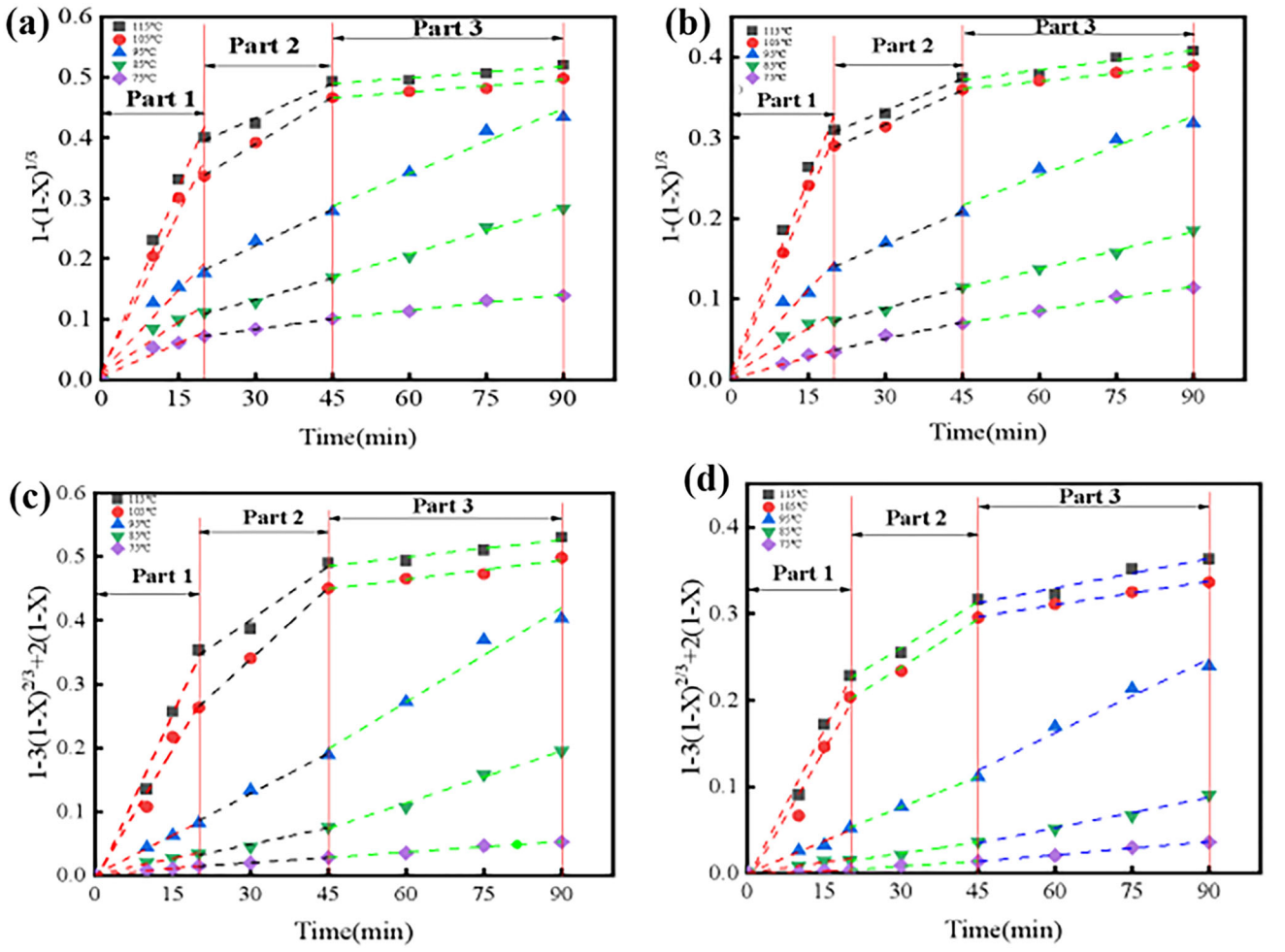

Fig. 5. Kinetic modeling of the dissolution of the laterite sample at temperatures from 75°C to 115°C. Left side: chemical control model (a) and internal diffusion model (c) for nickel. Right side: chemical control model (b) and internal diffusion model (d) for iron.

Table IV. Reaction rate constant and correlation coefficients at different temperatures for Ni and Fe dissolutions by chemical control model and internal diffusion model

	Ni				Fe			
	Chemical control model		Internal diffusion model		Chemical control model		Internal diffusion model	
Temperature (°C)	R^2	K (min^{-1})	R^2	K (min^{-1})	R^2	K (min^{-1})	R^2	K (min^{-1})
75 (Part1)	0.9903	0.00188	0.9813	6.6108E−4	0.9178	0.00142	0.9431	2.2460E−4
75 (Part2)	0.9999	0.00114	0.9988	5.4117E−4	0.9541	0.00137	0.9841	4.0679E−4
75 (Part3)	0.9820	8.9097E−4	0.9843	5.6410E−4	0.9920	0.00101	0.9954	5.0750E−4
85 (Part1)	0.9974	0.00307	0.9999	0.0014	0.8909	0.002	0.9054	7.1503E−4
85 (Part2)	0.9667	0.00221	0.9738	0.00171	0.9884	0.00167	0.9767	8.5819E−4
85 (Part3)	0.9936	0.0026	0.9925	0.00271	0.9767	0.00164	0.9850	0.00118
95 (Part1)	0.9987	0.00494	0.9999	0.00381	0.9312	0.00423	0.9138	0.00264
95 (Part2)	0.9800	0.00402	0.9908	0.00424	0.9960	0.00273	0.9997	0.00235
95 (Part3)	0.9626	0.00359	0.9676	0.00492	0.9881	0.00275	0.9727	0.00285
105 (Part1)	0.9334	0.0132	0.9483	0.01551	0.9501	0.01196	0.9912	0.01371
105 (Part2)	0.9990	0.0052	0.9997	0.00747	0.9974	0.0033	0.9935	0.00371
105 (Part3)	0.9517	6.7504E−4	0.9515	0.00101	0.9951	6.4679E−4	0.9956	9.0907E−4
115 (Part1)	0.9893	0.017	0.9918	0.0218	0.9773	0.01242	0.9886	0.01378
115 (Part2)	0.9724	0.00376	0.9417	0.00557	0.9915	0.00263	0.9894	0.00355
115 (Part3)	0.9278	6.1209E−4	0.8918	9.1779E−4	0.9393	8.0001E−4	0.9392	0.00114

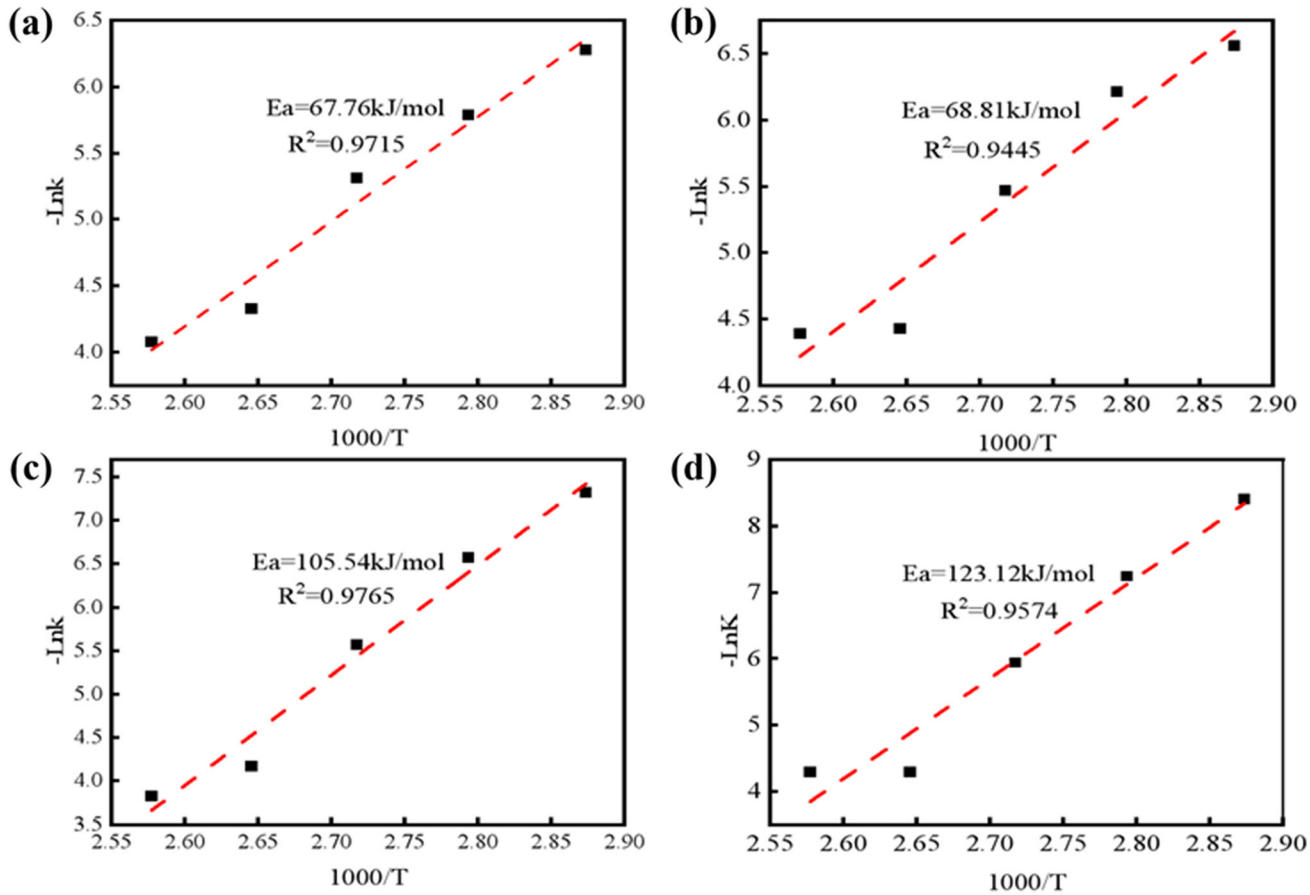

Fig. 6. The plot of -lnK versus 1000/T to calculate the activation energy. Left side: chemical control model (a) and internal diffusion model (c) for nickel. Right side: chemical control (b) model and internal diffusion model (d) for the iron.

Activation energies in excess of 40 kJ/mol indicate the effect of the reaction on the leaching behavior as determined by temperature and chemical control.

Figure 6c and d shows that the plots for nickel and iron in the internal diffusion control have acceptable correlation coefficients (R^2) of 0.9765 for nickel and 0.9574 for iron. For the internal diffusion control equations, the values of activation energies for the dissolution of nickel and iron are shown:

$$E_a = 105.54\ \text{kJ/mol}$$
$$E_a = 123.12\ \text{kJ/mol}$$

For diffusion-controlled processes, the previously reported low activation energies (< 24 kJ/mol) are 4–12 kJ/mol, 8–20 kJ/mol, and 12–24 kJ/mol.[15] Conversely, leaching processes with activation energies between 40 kJ/mol and 80 kJ/mol are regulated by surface chemical reactions.[30] It can be concluded that chemical control is more effective than diffusion control on the rate of laterite dissolution because the chemical control equations fit the laterite dissolution data at different temperatures well and the activation energies are within the range of the chemically controlled reaction.

Analysis of Leaching Residue

To explore the dissolution of each component during the leaching process of limonite-type laterite nickel ore, the leaching slag obtained at a leaching temperature of 115°C, a NH_4HSO_4 mass concentration of 75%, an excess rate of NH_4HSO_4 of 50%, and a leaching time of 90 min was selected for compositional and microstructural analysis. The chemical composition of the leaching slag is shown in Table V. After the extraction of nickel from limonite-type laterite nickel ore, the nickel content in the leaching slag decreased from 1.56% to 0.55%, the iron content decreased from 65.42% to 43.09%, and the SiO_2 content increased from 5.15% to 16.33%, resulting in a leaching rate of 88.96%. The main components of the leaching slag were analyzed using the XRD method. Figure 7a shows that the leaching slag is mainly composed of needle ferrite (FeO(OH)), hematite (Fe_2O_3), quartz (SiO_2), pyrophyllite ($Al_2Si_4O_{10}(OH)_2$), and spinel ($FeNiO_4$). The peak at 21.24° after leaching of acicular iron ore FeO(OH) decreased significantly, and the content of crystalline phase decreased, but most of the acicular iron ore (FeO(OH)) in the leaching slag not underwent a physical phase transition relative to the original ore, probably because the hydrolysis temperature that would enable it to produce hematite (Fe_2O_3) was not reached at the leaching temperature of 115°C. The leaching temperature of 115°C was not reached at the hydrolysis temperature of 115°C. The leaching temperature was not reached at the hydrolysis temperature that would enable it to produce hematite (Fe_2O_3). Hematite (Fe_2O_3) was still present in the leaching slag, indicating that acicular ferrite was more soluble relative to hematite, suggesting that the iron in solution was mainly derived from acicular ferrite. The micro-morphology of the untreated limonite-type nickel laterite leaching slag was observed by SEM. As shown in Fig. 7b and c, the surface of nickel laterite leaching slag is rough and uneven, and there are many tightly bound needle-like particles, indicating that part of the needle ferrite and nickel-iron oxides dissolved during the leaching of nickel laterite by ammonia hydrogensulfate solution. SEM is consistent with the results of XRD analysis, and there is a large reduction of nickel content by EDS in Fig. 7(c6) compared with the EDS analysis result of the original ore in Fig. 1(c5), which is consistent with the XRF analysis results. The shrinkage of the core of the unreacted laterite nickel ore until the nickel laterite particles are entirely dissolved in the liquid phase is shown by the notable reduction of nickel content in the leaching residue. The aforementioned analysis further implies that surface chemical processes regulate the leaching process of limonitic laterite nickel ore in ammonium bisulfate solution, based on the kinetic data of this study.

CONCLUSION

(1) The order of influence of process parameter on nickel leaching rate by using response surface methodology is leaching temperature > leaching time = acid concentration > acid excess rate. The optimal leaching conditions are 74% mass concentration of NH_4HSO_4, leaching time of 83 min, 17% excess rate of NH_4HSO_4, leaching temperature of 112°C, and the theoretical recovery of nickel is 90.9%.

(2) The optimal parameters of hydrogen sulfate ammonia leaching process obtained by the atmospheric pressure are 75% mass concentration of NH_4HSO_4, leaching time of 90 min, 50% excess of NH_4HSO_4, leaching temperature of 115°C, and the leaching yields of nickel and iron were 88.96% and 79.23%, respec-

Table V. Chemical composition of laterite nickel ore leaching residue (mass fraction, %)

Compound	Fe_2O_3	Al_2O_3	SiO_2	MgO	Cr_2O_3	NiO	MnO	Na_2O	Co_3O_4	Others	LOI
Wt.%	43.09	6.4	16.33	2.45	16.45	0.55	1.1	0.62	0.19	0.68	12.14

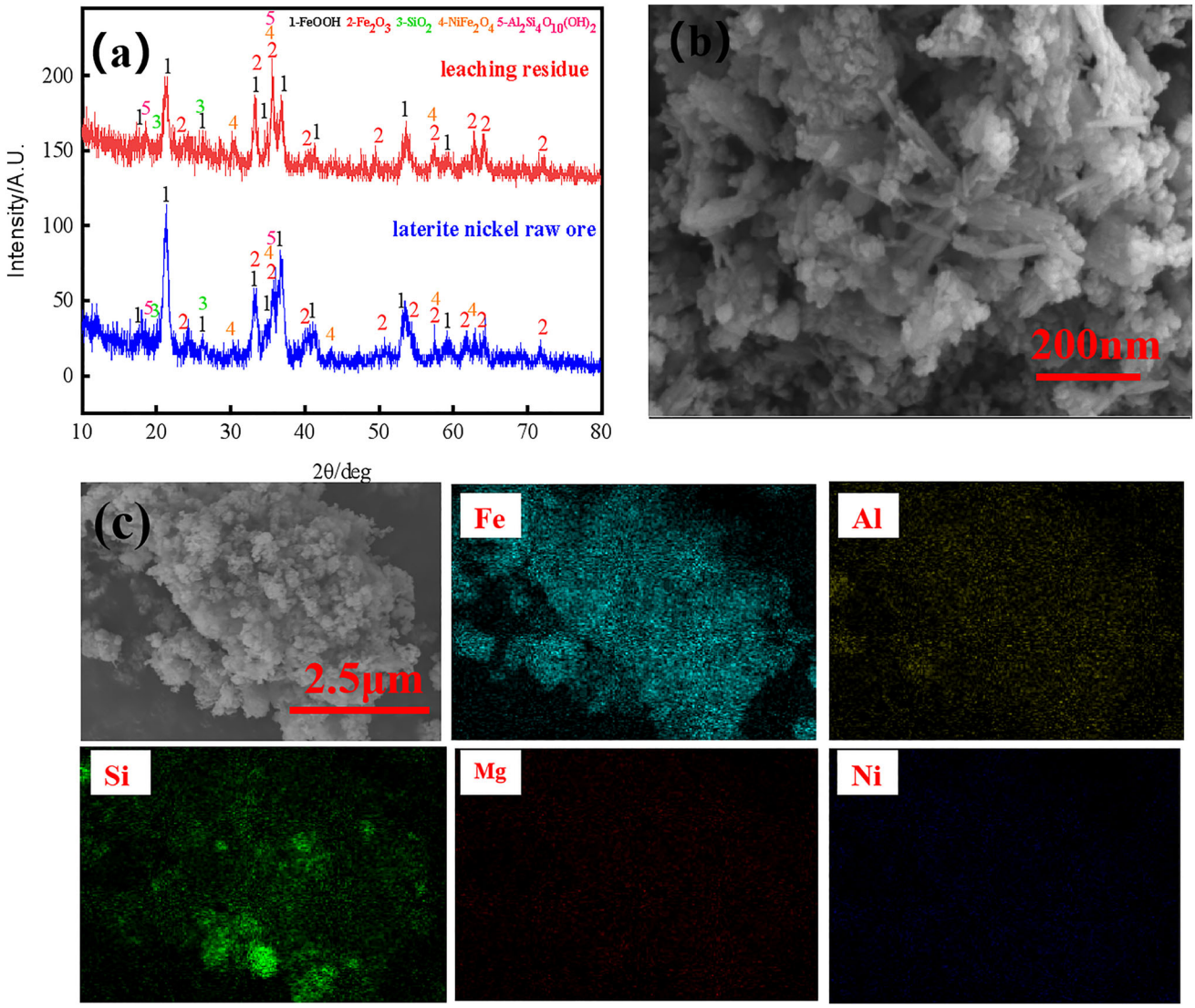

Fig. 7. Results of XRD (a) before and after leaching of laterite nickel ore, SEM images (b), and EDS (c) spectral analysis of after leaching of nickel laterite ore.

tively.

(3) The dissolution process of limonite type laterite nickel ore in ammonium bisulfate follows the shrinkage core model according to dynamic model analysis. The leaching rates of nickel and iron are controlled by the chemical reaction on the particle surface. The activation energies (E_a) of nickel and iron leaching are 67.76 kJ/mol and 68.81 kJ/mol, respectively.

SUPPLEMENTARY INFORMATION

The online version contains supplementary material available at https://doi.org/10.1007/s11837-024-06470-0.

ACKNOWLEDGEMENTS

This work is supported by the National Natural Science Foundation of China (Grant No. 51974188), the Liaoning Province Applied Basic Research Program Project 2023JH2/101300245, and the Liaoning Revitalization Talents Program (No. XLYC2008014).

CONFLICT OF INTEREST

On behalf of all authors, the corresponding author states that there is no conflict of interest.

REFERENCES

1. Z. Cao, B. Ma, J. Zhou, Y. Chen, and C. Wang, *Process Saf. Environ.* 168, 1 https://doi.org/10.1016/j.psep.2022.09.053 (2022).

2. Q.H. Tian, B. Dong, X.Y. Guo, Q.A. Wang, Z.P. Xu, and D. Li, *J. Cent. South Univ.* 30, 1776 https://doi.org/10.1007/s11771-023-5356-y (2023).
3. M.D. da Silva, M.R.D. Oliveira, I.D. dos Santos, P. Radino-Rouse, and M.B. Mansur, *Miner. Process. Extr. Metall. Rev.* 43, 28 https://doi.org/10.1080/08827508.2020.1809392 (2022).
4. C.K. Thubakgale, R.K.K. Mbaya, and K. Kabongo, *Miner. Eng.* 54, 79 https://doi.org/10.1016/j.mineng.2013.04.006 (2013).
5. D.H. Rubisov, J.M. Krowinkel, and V.G. Papangelakis, *Hydrometallurgy* 58, 1 https://doi.org/10.1016/s0304-386x(00)00094-3 (2000).
6. F. He, B. Ma, C. Wang, Y. Zuo, and Y. Chen, *Miner. Eng.* 185, 107671 https://doi.org/10.1016/j.mineng.2022.107671 (2022).
7. K.C. Wanta, W. Astuti, I. Perdana, and H.T.B.M. Petrus, *Minerals* 10, 613 https://doi.org/10.3390/min10070613 (2020).
8. Q. Guo, J. Qu, B. Han, P. Zhang, Y. Song, and T. Qi, *Miner. Eng.* 71, 1 https://doi.org/10.1016/j.mineng.2014.08.010 (2015).
9. M.A.R. Onal and Y.A. Topkaya, *Hydrometallurgy* 142, 98 https://doi.org/10.1016/j.hydromet.2013.11.011 (2014).
10. J. Li, Y. Yang, Y. Wen, W. Liu, Y. Chu, R. Wang, and Z. Xu, *Minerals* 10, 745 https://doi.org/10.3390/min10090754 (2020).
11. J.H. Li, D.S. Li, Z.F. Xu, C.F. Liao, Y. Liu, and B. Zhong, *J. Clean. Prod.* 179, 24 https://doi.org/10.1016/j.jclepro.2018.01.085 (2018).
12. J.H. Li, Z.F. Xu, R.X. Wang, Y. Gao, and Y. Yang, *Physicochem. Probl. Miner. Process.* 55, 711 https://doi.org/10.5277/ppmp18189 (2019).
13. M.H. Nasab, M. Noaparast, and H. Abdollahi, *Int. J. Chem. Kinet.* 52, 283 https://doi.org/10.1002/kin.21349 (2020).
14. G. Prameswara, Y.P.T. Flaviana, P. Monita, T. Iga, and T.B.M.P. Himawan, *Trans. Indian Inst. Met.* 76, 1341 https://doi.org/10.1007/s12666-022-02858-1 (2023).
15. J. MacCarthy, A. Nosrati, W. Skinner, and J. Addai-Mensah, *Hydrometallurgy* 160, 26 https://doi.org/10.1016/j.hydromet.2015.11.004 (2016).
16. X.Y. Guo, W.T. Shi, D. Li, and Q.H. Tian, *Trans. Nonferr. Met. Soc. China* 21, 191 https://doi.org/10.1016/s1003-6326(11)60698-5 (2011).
17. E. Buyukakinci and Y.A. Topkaya, *Hydrometallurgy* 97, 33 https://doi.org/10.1016/j.hydromet.2008.12.014 (2009).
18. K. Yan, L. Liu, H. Zhao, L. Tian, Z. Xu, and R. Wang, *Front. Chem.* 8, 592837 https://doi.org/10.3389/fchem.2020.592837 (2021).
19. Y.S. Wu, X. Yang, L.S. Li, Y.Z. Wang, and M.C. Li, *Chem. Pap.* 73, 2289 https://doi.org/10.1007/s11696-019-00779-w (2019).
20. W. Li, L.S. Li, Y.S. Wu, Y.Z. Wang, M.C. Li, and Z.Q. Ning, *JOM* 75, 4385 https://doi.org/10.1007/s11837-023-06058-0 (2023).
21. K. Liu, Y. Wang, H. Long, Y.F. Cheng, Y. Wu, Y.Z. Cai, and J.T. Jiang, *Miner. Eng.* 169, 106961 https://doi.org/10.1016/j.mineng.2021.106961 (2021).
22. W. Astuti, F. Nurjaman, F.R. Mufakhir, S. Sumardi, D. Avista, K.C. Wanta, and H. Petrus, *Miner. Eng.* 191, 107982 https://doi.org/10.1016/j.mineng.2022.107982 (2023).
23. R.H. Myers, D.C. Montgomery, G.G. Vining, C.M. Borror, and S.M. Kowalski, *J. Qual. Technol.* 36, 53 https://doi.org/10.1080/00224065.2004.11980252 (2004).
24. M.A. Bezerra, R.E. Santelli, E.P. Oliveira, L.S. Villar, and L.A. Escaleira, *Talanta* 76, 965 https://doi.org/10.1016/j.talanta.2008.05.019 (2008).
25. Ž. R. Lazić, *Design of Experiments in Chemical Engineering A Practical Guide* (Weinhem, Euros, 2005), p. 610. https://doi.org/10.1002/3527604162.
26. L. Panda, D.S. Rao, B.K. Mishra, and B. Das, *Min. Metall. Explor.* 31, 57 https://doi.org/10.1007/BF03402349 (2014).
27. P.Y. Zhang, G. Qiang, J.K. Qu, and Q. Tao, *Russ. J. Non-Ferr. Met.* 61, 42 https://doi.org/10.3103/s1067821220010113 (2020).
28. C.A.J. Tupaz, Y. Watanabe, K. Sanematsu, and T. Echigo, *Ore Geol. Rev.* 125, 103686 https://doi.org/10.1016/j.oregeorev.2020.103686 (2020).
29. X.M. Lv, W. Lv, Z.X. You, X.W. Lv, and C.G. Bai, *Powder Technol.* 340, 495 https://doi.org/10.1016/j.powtec.2018.09.061 (2018).
30. J. MacCarthy, A. Nosrati, W. Skinner, and J. Addai-Mensah, *Powder Technol.* 286, 420 https://doi.org/10.1016/j.powtec.2015.07.013 (2015).